

Global nitrous oxide production determined by oxygen sensitivity of nitrification and denitrification

Qixing Ji^{1†}, Erik Buitenhuis², Parvatha Suntharalingam², Jorge L. Sarmiento³ and Bess B. Ward¹

¹Department of Geosciences, Guyot Hall, Princeton University, Princeton, New Jersey, 08540, United States of America.

²School of Environmental Science, University of East Anglia, Norwich Research Park, Norwich, Norfolk, NR4 7TJ, United Kingdom.

³Program in Atmospheric and Oceanic Sciences, Princeton University, Princeton, New Jersey, 08540, United States of America.

Corresponding author: Qixing Ji (qji@alumni.princeton.edu)

† Current address: Helmholtz Centre for Ocean Research Kiel, Düsternbrooker Weg 20, 24105, Kiel, Germany.

Key Points:

- New quantitative relationships between oxygen and nitrous oxide production are derived from direct measurements in low oxygen oceans
- The presence of oxygen reduces nitrous oxide production via nitrification and denitrification
- The latest biogeochemical model incorporating the field measurements and relationships provides new estimate of global marine nitrous oxide flux

This article has been accepted for publication and undergone full peer review but has not been through the copyediting, typesetting, pagination and proofreading process which may lead to differences between this version and the Version of Record. Please cite this article as doi: 10.1029/2018GB005887

Abstract

The ocean is estimated to contribute up to ~20% of global fluxes of atmospheric nitrous oxide (N₂O), an important greenhouse gas and ozone depletion agent. Marine oxygen minimum zones (OMZs) contribute disproportionately to this flux. To further understand the partition of nitrification and denitrification and their environmental controls on marine N₂O fluxes, we report new relationships between oxygen concentration and rates of N₂O production from nitrification and denitrification directly measured with ¹⁵N tracers in the Eastern Tropical Pacific. Highest N₂O production rates occurred near the oxic-anoxic interface, where there is strong potential for N₂O efflux to the atmosphere. The dominant N₂O source in OMZs was nitrate reduction, the rates of which were one to two orders of magnitude higher than those of ammonium oxidation. The presence of oxygen significantly inhibited the production of N₂O from both nitrification and denitrification. These experimental data provide new constraints to a multi-component global ocean biogeochemical model, which yielded annual oceanic N₂O efflux of 1.7 – 4.4 Tg-N (median 2.8 Tg-N, 1 Tg = 10¹² g), with denitrification contributing 20% to the oceanic flux. Thus, denitrification should be viewed as a net N₂O production pathway in the marine environment.

1 Introduction

The unprecedented rate of increase in atmospheric nitrous oxide (N₂O) concentration since the Industrial Revolution (Blasing, 2016) is alarming because N₂O is a strong greenhouse gas and, following the successful mitigation of halocarbons, will be the most important ozone depletion agent by the end of the 21st century (Ravishankara *et al.*, 2009). N₂O from soil, coastal waters and the open ocean is emitted into the troposphere, where N₂O is chemically inert, resulting in the pronounced increase of N₂O burden. The average lifetime of N₂O in the atmosphere is estimated to be more than 100 years (Prather *et al.*, 2012); photolytic destruction in the stratosphere is the major sink. Intense N₂O emissions in the open ocean occur in upwelling regions where oxygen minimum zones (OMZs) are located (Codispoti, 2010). OMZs are characterized by sharp oxygen (O₂) gradients (oxycline strength >2.5 μmol L⁻¹ m⁻¹) overlying an anoxic layer of hundreds of meters in depth. Extreme N₂O supersaturation with respect to the atmosphere occurs in the oxycline, indicating active N₂O production and the potential for efflux to the atmosphere (Elkins *et al.*, 1978; Codispoti and Christensen, 1985; Law and Owens, 1990). Although the OMZs occupy

< 1% of the ocean volume (Codispoti *et al.*, 2001), they potentially contribute up to 50% of marine N₂O efflux (Codispoti, 2010). The Intergovernmental Panel on Climate Change (IPCC) reports that the ocean contributes 3.8 Tg-N yr⁻¹ (1 Tg = 10¹² g), ~ 21 % of the total N₂O emissions (Ciais *et al.*, 2013). However, incomplete understanding of marine N₂O production pathways and their sensitivities to environmental factors resulted in large uncertainties of current N₂O emission estimates (1.8 – 9.4 Tg-N yr⁻¹), and limited our ability to predict future N₂O emission under the changing ocean and climate (Landolfi *et al.*, 2017; Battaglia and Joos, 2018).

Biological N₂O production in the ocean is attributed to ammonium (NH₄⁺) oxidation, nitrite (NO₂⁻) reduction and nitrate (NO₃⁻) reduction (Figure 1). During aerobic NH₄⁺ oxidation to NO₂⁻, the first step in nitrification (by both bacteria and archaea), N₂O is emitted as a byproduct, with higher N₂O yield (the molar nitrogen ratio of N₂O to NO₂⁻ production) at lower O₂ conditions (Goreau *et al.*, 1980; Löscher *et al.*, 2012). Under low O₂ and anoxic conditions, NO₃⁻ and NO₂⁻ can be reduced to N₂O through stepwise conventional denitrification (NO₃⁻ → NO₂⁻ → NO → N₂O), with organic matter as the electron donor. Nitrite reduction, which occurs in O₂ conditions from fully saturated to functional anoxia (Frame and Casciotti, 2010), is mediated by both nitrifiers (Poth and Focht, 1985) and denitrifiers (Cohen and Gordon, 1978). ‘Nitrifier denitrification’ refers to NO₂⁻ reduction to N₂O in oxygenated water column where conventional denitrification is insignificant (Wilson *et al.*, 2014). In the OMZs, the sharp O₂ gradient provides niches for both nitrifying and denitrifying organisms to enable N₂O production from both nitrification and denitrification (Codispoti and Christensen, 1985). In this study, ‘nitrification’ refers to NH₄⁺ oxidation whereas ‘denitrification’ refers to NO₃⁻ and NO₂⁻ reduction. At present, distinguishing nitrifier denitrification from conventional denitrification (i.e. both can conduct

NO_2^- reduction to N_2O) in natural environments is difficult due to the lack of reliable methodology.

Nitrification is regarded as the main pathway of global oceanic N_2O production because denitrification is mainly restricted to OMZs and because N_2O consumption is assumed to dominate over N_2O production by denitrification in the OMZs (Codispoti, 2010; Freing *et al.*, 2012). This notion was challenged by recent observations and model analysis (Babbin *et al.*, 2015; Ji *et al.*, 2015; Bourbonnais *et al.*, 2017), which suggested high rates of N_2O production from NO_3^- reduction in the OMZs. Lacking reliable quantification of nitrogen cycling processes in OMZs, previous biogeochemical models predominantly employed simple parameterizations representing N_2O production derived from limited culture analyses and in-situ measurements, and model analysis of the relative contribution of N_2O production from denitrification and nitrification to the total oceanic flux is uncertain (Suntharalingam *et al.*, 2012; Battaglia and Joos, 2018).

We applied nitrogen stable isotope (^{15}N) incubation experiments to directly measure rates and pathways of N_2O production in the OMZs of the Eastern Tropical South and North Pacific (ETSP and ETNP). To evaluate control of N_2O production by oxygen, we derived quantitative relationships between oxygen concentration and N_2O production from NH_4^+ oxidation, NO_2^- and NO_3^- reduction. The rate distribution and O_2 relationships were incorporated into a multi-component ocean biogeochemistry and ecosystem model to estimate global oceanic N_2O fluxes, and to partition the contributions of the nitrification and denitrification pathways.

2 Methods

2.1 Shipboard Sampling

Shipboard sampling and incubation experiments were carried out on the *R/V Atlantis* during January, 2015 (Cruise ID: AT26-26); and *R/V Ronald H. Brown* during April 2016 (Cruise ID: RB1603). Samples were collected from the North (15°N – 20°N) and South Pacific (10°S – 20°S) coastal upwelling zones off the coast of Mexico and Peru (Figure 2). Stations were chosen to represent coastal environment (<100 nautical miles from the coast) and open-ocean environment (>200 nautical miles from the coast). Water was collected in 12 L Niskin bottles mounted on a standard conductivity-temperature-depth (CTD) rosette system. During the 2015 cruise, an oxygen sensor (Seabird SBE43, Bellevue, WA) calibrated by Winkler titration (detection limit 0.7 – 2.5 $\mu\text{mol kg}^{-1}$), and a real-time STOX sensor (detection limit 10 nmol L^{-1} (Revsbech *et al.*, 2009)) were deployed on the CTD. During the 2016 cruise, only the Seabird oxygen sensor was deployed. Dissolved inorganic nitrogen species (NH_4^+ , NO_2^- and NO_3^-) were measured onboard: NH_4^+ was measured fluorometrically by reaction with orthophthaldialdehyde (OPA) (Holmes *et al.*, 1999); NO_2^- was measured using a colorimetric method (Hansen and Koroleff, 1999) and $\text{NO}_3^- + \text{NO}_2^-$ was measured using cadmium reduction protocols established by UNESCO (UNESCO, 1994). See Figure S1 for typical profiles of oxygen and inorganic nitrogen during ETSP 2015 and ETNP 2016. Physical and chemical data from the ETSP in 2013 were described previously (Ji *et al.*, 2015).

2.2 N_2O production rate measurements

Incubation experiments to measure N_2O production using ^{15}N tracers were targeted at depths with water column features including the surface mixed layer, the base of the euphotic layer, local $[\text{NO}_2^-]$ maxima, sharp oxygen gradients (oxycline) and oxic-anoxic interfaces. Seawater was sampled from 12 L Niskin bottles into the bottom of acid washed, 60-mL glass serum bottles (Catalog# 223745, Wheaton, USA) and then allowed to overflow two to three

times the volume before sealing the bottles with butyl septa and aluminum rings. To facilitate tracer addition, as well as compensating for oxygen contamination from air, helium headspace (3 mL) was created. Three suites of ^{15}N tracer solutions ($^{15}\text{NH}_4^+$ plus $^{14}\text{NO}_2^-$, $^{15}\text{NO}_2^-$ plus $^{14}\text{NH}_4^+$, $^{15}\text{NO}_3^-$ plus $^{14}\text{NH}_4^-$ and $^{14}\text{NO}_2^-$) were applied to enrich $^{15}\text{NH}_4^+$, $^{15}\text{NO}_2^-$ and $^{15}\text{NO}_3^-$ to 0.2, 0.4 and 0.4 $\mu\text{mol L}^{-1}$ (final concentration), respectively; and increase concentrations of $^{14}\text{NH}_4^+$, $^{14}\text{NO}_2^-$ or $^{14}\text{NO}_3^-$ by 0.2, 0.4 and 0.4 $\mu\text{mol L}^{-1}$ (μM), respectively. Most of the samples had *in situ* concentrations of NH_4^+ below 0.02 μM (Figure S1) and thus rates of N_2O and NO_2^- production from NH_4^+ should be treated as potential rates. Samples for incubation experiments, except for one surface sample (10 m), had *in situ* NO_3^- concentrations > 4.6 μM ; samples collected from the ODZ and outside the ODZ generally had *in situ* NO_2^- concentrations > 1 μM and < 0.1 μM , respectively (see supplementary dataset). Tracer solutions were made from deionized water, and were flushed with helium gas before adding 0.1 mL into each sample. Incubations lasted 12 – 18 hours in temperature-controlled chambers ($\pm 2^\circ\text{C}$ of *in situ* temperature), during which duplicate samples were preserved every 6 – 9 hours (3 time points in total) with 0.1 mL saturated mercuric chloride (HgCl_2). Dilution of ^{15}N -labeled species were considered insignificant due to short incubation time.

The effect of oxygen concentrations on N_2O production was further investigated in the top of the anoxic layer (*in situ* $[\text{O}_2]$ < 0.1 μM verified by STOX sensor). During the 2015 ETSP cruise, the depths were 160 m and 80 m at offshore and coastal stations, respectively. During the 2016 ETNP cruise, the interface was at 188 m and 89 m at offshore and coastal stations, respectively. Samples were acquired using a pump profiling system (PPS) equipped with a CTD package, an oxygen sensor (SBE-25, Seabird Electronics, Bellevue, WA), and a real-time STOX unit. The PPS minimized oxygen contamination during sampling and allowed better representation of *in situ* anoxic conditions during incubation experiments. The

serum bottles were filled directly from the pump outlet and sealed without a headspace with septa and aluminum rings. Then, 3.2, 3.5, 4.0, 5.0, 8.0 mL helium headspace was created, volumes of 0.2, 0.5, 1.0, 2.0 and 5.0 mL of O₂ saturated site water (~225 μM) were injected into the incubation bottles to attain 0.3, 0.7, 1.4, 2.8 and 7 μM dissolved [O₂] (calculated by assuming equilibrium between the water phase and 3.0 mL final headspace in the incubation bottles (Garcia and Gordon, 1992)). The same suite of tracers as above was utilized. Incubation lasted 12 – 18 hours at ±2 °C of *in situ* temperatures, during which duplicate samples were preserved every 6 – 9 hours (3 time points in total) with 0.1 mL saturated HgCl₂.

Upon return to the home laboratory, N₂O in the water and headspace was stripped from the samples and analyzed using an autosampler in line with a cryo-focusing unit with helium as carrier gas, and injected into a Thermo-Finnigan Delta V for N₂O concentration and isotope ratio (m/z = 44, 45, 46) measurements. N₂O concentration was calculated from the amount of N₂O detected by mass spectrometry divided by the volume of seawater in the serum bottles (calibrated as 56.5 ± 0.1 mL). N₂O production was calculated from the progressive increase in mass 45 and 46 N₂O (⁴⁵N₂O and ⁴⁶N₂O) in time course experiments.

Equation (1)
$$R = \frac{1}{F} \times \left(\frac{d^{45}N_2O}{dt} + 2 \times \frac{d^{46}N_2O}{dt} \right)$$

where $d^{45}N_2O/dt$ and $d^{46}N_2O/dt$ represent the production rates of during incubation of ⁴⁵N₂O and ⁴⁶N₂O. F represents the ¹⁵N atom fraction in the initial substrate pool (NH₄⁺, NO₂⁻, and NO₃⁻). Rates were considered significant if the linear regression of the time course data having p<0.05 (n=5, ANOVA).

2.3 NO₂⁻ production measurements

After samples were analyzed for N₂O production, samples spiked with ¹⁵NH₄⁺ were also assayed for ¹⁵NO₂⁻ to determine N₂O yield during nitrification. 3 mL of each sample was

transferred using a 5-mL gas-tight glass syringe (Hamilton Co., Reno, NV, USA) from the 60-mL serum bottle to a helium-flushed 20-mL glass vial (Catalog# C4020-25, Thermo Fisher Scientific, Waltham, MA). Dissolved $^{15}\text{NO}_2^-$ was converted to N_2O using the acetic acid-treated sodium azide solution for quantitative conversion (McIlvin and Altabet, 2005). Resulting N_2O was measured on the Thermo-Finnigan Delta V for isotope ratio measurements.

2.4 Data Analysis

All data were deposited in Microsoft Excel® for statistical analysis and figure production. Oxygen profiles (1 meter binned-average from the CTD data package) were computed as the 5 meter moving average. The depth of the oxic-anoxic interface was determined as the depth below the oxycline at which the standard deviation of the moving-averaged oxygen concentrations became $< 0.1 \mu\text{mol kg}^{-1}$.

2.5 Three-dimensional marine N_2O production simulation

The prognostic global ocean general circulation Nucleus for European Modelling of the Ocean (NEMO) v3.1 model (Madec *et al.*, 1998) was forced by daily meteorological data from the National Centers for Environmental Prediction (NCEP) reanalysis. Embedded in the ocean circulation model, biogeochemistry was simulated by the PlankTOM10 model (Le Quéré *et al.*, 2016; Buitenhuis *et al.*, 2018). The NEMO-PlankTOM10 system has a horizontal resolution of 2° with higher resolution (up to 0.5°) in tropical and polar latitudes. There are 31 vertical levels in the entire water column and 10 m resolution in the upper 100 m. The oxygen distribution in the ocean was fixed according to the reanalysis of the World Ocean Atlas oxygen dataset, which had minimum $[\text{O}_2] > 1 \mu\text{M}$ (Bianchi *et al.*, 2012). The export production was estimated to be 5.8 PgC yr^{-1} , consistent with recent model estimates (Siegel *et al.*, 2014; Bisson *et al.*, 2018). The NEMO-PlankTOM10 system

simulates the rates of nitrogen remineralization and N₂O production by relating oxygen consumption and organic matter remineralization below the euphotic zone:

Equation (2)

[Oxygen Consumption Rate] = respiration by the 10 model plankton functional types (6 phytoplankton, 3 zooplankton and picoheterotrophs (*Bacteria* + *Archaea*))

Equation (3)

[Nitrogen remineralization rate] = [Oxygen Consumption Rate] × (16 mol N / 172 mol O₂) (Takahashi *et al.*, 1985)

Parameterization of N₂O production was modified from previous model setup (Suntharalingam *et al.*, 2012; Capelle *et al.*, 2018) so as to employ *in situ* oxygen concentrations to compute N₂O production from nitrification and denitrification:

Equation (4)

N₂O Source = $J_1 + J_2$

$J_1 = [a / [O_2] (\mu\text{M}) + b] \times 0.01 \times [\text{Nitrogen remineralization rate}]$

$J_2 = \beta \times f(O_2) \times [\text{Nitrogen remineralization rate}]$

The two separate terms (J_1 and J_2) represent (a) NH₄⁺ oxidation to N₂O in the presence of oxygen (J_1), which is parameterized according to an empirical relationship between N₂O yield and *in situ* O₂ concentrations during NH₄⁺ oxidation (see section 3.1 and Figure 4); and (b) the enhanced N₂O production via NO₂⁻ and NO₃⁻ reduction in OMZs (J_2). The linear scaling parameter β is derived from Suntharalingam *et al.* (2012), which represents increased N₂O production from denitrification in suboxic conditions; and is set at 0.215, meaning up to 0.215 mol N₂O-N is produced when 1 mol of nitrogen is remineralized. The function $f(O_2)$ accounts for the functional dependence of N₂O yield on oxygen level.

Equation (5)

$f(O_2) = \exp(\lambda ([O_2] - [O_{2\text{-offset}}]))$ when $[O_2] > [O_{2\text{-offset}}]$

$f(O_2) = [O_2] / [O_{2\text{-offset}}]$ when $[O_2] < [O_{2\text{-offset}}]$

The $[O_{2\text{-offset}}]$ represents the oxygen concentration below which net N₂O production is reduced due to N₂O consumption by denitrification, and is set to 1 μM (Dalsgaard *et al.*,

2014; Capelle *et al.*, 2018). The effect of O₂ on N₂O production from denitrification (NO₂⁻ and NO₃⁻ reduction) was experimentally measured (see section 3.2) to determine the parameterization of λ (see section 3.3 and Table 1).

The evolution of the atmospheric N₂O partial pressure since the Industrial Revolution is parameterized as:

$$\text{Equation (6)} \quad pN_2O_{\text{atm}} = 0.000009471353 \times Y^3 - 0.05214714 \times Y^2 + 95.68066 \times Y - 58228.41$$

in which pN_2O_{atm} is in natm and Y is the decimal year (Buitenhuis *et al.*, 2018, as corrected from Freing *et al.*, 2009). Oceanic N₂O flux to the atmosphere (F) is computed as the product of gas transfer velocity (k) and the difference between model-derived surface ocean concentration (C_s) and equilibrium concentration (C_{eq}):

$$\text{Equation (7)} \quad F = k \times (C_s - C_{\text{eq}})$$

The C_{eq} is computed following the equations of N₂O solubility in seawater with in situ temperature, salinity and pN_2O_{atm} (Weiss and Price, 1980). Daily NCEP wind product (U) and Schmidt number for N₂O (Sc) is used to calculate the gas transfer velocity k (Wanninkhof, 1992).

$$\text{Equation (8)} \quad k = 0.31U^2 (Sc/660)^{-0.5}$$

Model spin-up was performed to reach steady state of N₂O concentration. Thus water column N₂O production approximated to the oceanic flux. Statistical comparison of simulated N₂O distribution pattern both at the surface and depth were performed (Figure S2) with respect to observations compiled in the MEMENTO database (Kock and Bange, 2015).

3 Results

Rates of N_2O production from NH_4^+ oxidation (Figure 3A), NO_2^- reduction (Figure 3B) and NO_3^- reduction (Figure 3C) were relatively higher across the oxic-anoxic interface compared to depths > 100 m deeper or shallower than the interface in the Eastern North and South Pacific OMZs. Highest rates of N_2O production from NH_4^+ oxidation, NO_2^- and NO_3^- reduction were detected close to (± 50 m) the oxic-anoxic interface. Rates were very low at depths ≥ 200 m below the oxic-anoxic interface and in the oxygenated layer ≥ 100 m above the interface. The rates of N_2O production from nitrification and denitrification, and their control by environmental factors are presented below.

3.1 N_2O production in the OMZs

For N_2O production from NH_4^+ oxidation, maximum rates (up to $0.05 \text{ nmol-N L}^{-1} \text{ d}^{-1}$) were detected within 100 m above the oxic-anoxic interface (Figure 3A). This depth range within 100 m above the interface generally corresponds to the oxycline and N_2O supersaturation (data not shown). In the oxygenated layer, the majority of the rate measurements were $0 - 0.02 \text{ nmol-N L}^{-1} \text{ d}^{-1}$, and the rates decreased at shallower depths. In the anoxic layer below the interface, NH_4^+ oxidation is inhibited by anoxia, resulting in very low or undetectable rates of N_2O production from NH_4^+ oxidation. At deeper depths (≥ 200 m below the oxic-anoxic interface), N_2O production rates from NH_4^+ oxidation were very slow ($< 0.001 \text{ nmol-N L}^{-1} \text{ d}^{-1}$). Direct measurement of N_2O yield in natural waters under a range of O_2 conditions (Figure 4) was achieved by the simultaneous measurements of N_2O and NO_2^- production from NH_4^+ oxidation. Consistent with elevated rates of N_2O production from NH_4^+ oxidation close to the oxic-anoxic interface, the N_2O yield increased non-linearly from $0.003 - 0.06 \%$ at $> 50 \mu\text{M O}_2$, to higher than 2% at $< 0.5 \mu\text{M O}_2$. Particularly at O_2 concentration $< 5 \mu\text{M}$, significant increase of yield up to two orders of magnitude, was observed with decreasing O_2 concentration. An empirical fit between N_2O yield (%) from nitrification and O_2 concentration (μM) was derived: $\text{Yield} = (0.2 \pm 0.13) / [\text{O}_2] + (0.08 \pm 0.04)$,

$r^2 = 0.33$. This relationship implies that (1) the range of N_2O yield during nitrification at 0.1 – 300 μM O_2 concentrations is 0.04 – 3 %; (2) outside of the OMZ at $> 50 \mu\text{M}$ O_2 , the uncertainty range of the yield is 0.04 – 0.12 %. Compared to previous studies relying on cultured AOB for yield measurements (Goreau *et al.*, 1980; Nevison *et al.*, 2003), natural waters from the OMZs have 10 – 100 fold lower yield at O_2 concentrations $< 10 \mu\text{M}$ (Figure 4). Within the oxycline where the O_2 concentration generally varies between 10 and 100 μM , the N_2O yield measurements of natural waters are 2 – 10 fold lower than those from cultured AOB.

N_2O production from both NO_2^- and NO_3^- reduction was detected in the oxycline, generally within 30 m above the oxic-anoxic interface and in the anoxic depths (Figures 3B - C). Highest rates (up to 2 $\text{nmol-N L}^{-1} \text{d}^{-1}$) were detected within the oxycline and were 10 – 100-fold higher than N_2O production from NH_4^+ oxidation. The majority of rates of NO_2^- reduction to N_2O ranged from 0 – 1.5 $\text{nmol-N L}^{-1} \text{d}^{-1}$, except for one measurement of 6.8 $\text{nmol-N L}^{-1} \text{d}^{-1}$ (Figure 3B). Highest rates of N_2O production from NO_2^- and NO_3^- reduction occurred just below the oxic-anoxic interface. Both NO_2^- and NO_3^- are substrates for denitrifiers producing N_2O . However, in most paired samples, rates of N_2O production from NO_3^- reduction were 2 – 7-fold higher than N_2O production from NO_2^- reduction; the median contribution of NO_3^- reduction to total N_2O production from denitrification is 73%. The relative magnitude of the two rates may be related to the ratio of NO_2^- and NO_3^- concentrations (Figure 5). The linear regressions between the ratio of N_2O production rates from NO_2^- vs. from NO_3^- , and the concentration ratio of $[\text{NO}_2^-]/[\text{NO}_3^-]$ are as follows: Within concentration ratio of 0 – 0.5, $y = 0.5066x + 0.0137$, $r^2=0.43$, $p = 0.00015$ (ANOVA, $n=28$); within concentration ratio of 0 – 2.0, $y = 0.3025x + 0.0625$, $r^2=0.896$, $p = 1\text{E-}15$ (ANOVA, $n=30$).

3.2 Effects of Oxygen on N₂O production

The effects of elevated O₂ (0 – 7 μM) on N₂O production from NH₄⁺ oxidation, NO₂⁻ reduction and NO₃⁻ reduction were experimentally investigated at the oxic-anoxic interface in both coastal and offshore waters (Figure 6). Under *in situ* O₂ concentration (< 0.1 μM), coastal stations had higher rates of N₂O production from NH₄⁺ oxidation, NO₂⁻ reduction and NO₃⁻ reduction. An exception was that, during 2015 ETSP cruise, similar rates of NO₂⁻ reduction to N₂O in coastal and offshore stations were observed (0.45 nmol-N L⁻¹ d⁻¹, Figure 6B). Highest rates of N₂O production from NH₄⁺ and NO₂⁻ were measured under *in situ* O₂ concentration. These rates were significantly reduced during the course incubation experiments (within a day) in the presence of > 1 μM O₂. At 7 μM O₂, rates of N₂O production from NH₄⁺ and NO₂⁻ were reduced by 50 – 100 % (Figures 6A and 6B). The NO₂⁻ data were fitted with exponential-type inhibition kinetics [inhibition = 1 – exp (-k × O₂ (μM))] to derive half inhibition O₂ concentration (C₅₀ = -ln(0.5)/k). The C₅₀ for NO₂⁻ reduction to N₂O in the ETSP and ETNP at both coastal and offshore stations was 1.5 ± 0.9 μM (p = 0.01). By contrast, increasing O₂ concentration up to 7 μM was ineffective to inhibit N₂O production from NO₃⁻ reduction during the 18-hour long incubations (Figure 6C). At the coastal and offshore stations, the range of rates was 0.8 – 1.2 nmol-N L⁻¹ d⁻¹ and 0 – 0.13 nmol-N L⁻¹ d⁻¹, respectively. Statistical fit of the C₅₀ for NO₃⁻ reduction to N₂O was 14 ± 4 μM (p = 0.08).

3.3 Global oceanic N₂O production

A three-dimensional ocean biogeochemical model incorporating our new data on N₂O production pathways and their sensitivities to oxygen, was used to estimate marine N₂O production and oceanic efflux on the global scale. With the formulation of N₂O yield during nitrification as a function of O₂ concentration (Yield (%) = 0.2 / [O₂] (μM) + 0.08, Figure 4), global marine N₂O efflux from nitrification was estimated as 2.2 Tg-N yr⁻¹. The contribution

from nitrification is small in the OMZs ($< 0.05 \text{ Tg-N yr}^{-1}$). The uncertainty of N_2O production from nitrification ($1.1 - 3.3 \text{ Tg-N yr}^{-1}$, simulation 2 and 3, Table 1) was derived from the parameters' uncertainties of nitrification N_2O yield ($\text{Yield} = (0.2 \pm 0.13) / [\text{O}_2] + (0.08 \pm 0.04)$). To estimate the range of N_2O production from denitrification, the varying sensitivities of O_2 inhibition on NO_2^- and NO_3^- reduction to N_2O were considered, which were formulated as the rates decreasing by $1/e$ ($\sim 36.8\%$) for 1.5 (lower boundary), 10 (median) and 20 μM (upper boundary) of O_2 increase, corresponding to $\lambda = -0.6667, -0.1$ and -0.05 for Equation (6) (Table 1, simulation 1, 4 and 5). Thus, net N_2O production from denitrification ranged $0.1 - 2.1 \text{ Tg-N yr}^{-1}$, with the median estimate of 0.6 Tg-N yr^{-1} . Summarizing the above sensitivity analyses, we estimate global oceanic N_2O efflux of 2.8 Tg-N yr^{-1} (range $1.7 - 4.4 \text{ Tg-N yr}^{-1}$, Table 1), with denitrification across the oxic-anoxic interface in OMZs contributing $\sim 20\%$ of the total fluxes.

Intense marine N_2O fluxes, $0.01 - 0.12 \text{ g N m}^{-2} \text{ yr}^{-1}$ (equivalent to $0.9 - 9 \text{ mmol-N m}^{-2} \text{ yr}^{-1}$) occur in the Eastern Tropical Pacific (Figure 7). The high latitude oceans, e.g. the sub-Arctic North Atlantic and the Southern Ocean, are sites with moderate N_2O fluxes. In contrast, the fluxes were negligible in the subtropical gyres in the North and South Pacific, the North Atlantic and South Indian Oceans.

4 Discussion

4.1 Oxidative vs. reductive N_2O production pathways

The Eastern tropical Pacific is regarded as a “hot spot” of N_2O production because of water column N_2O supersaturation near the oxic-anoxic interface. The presence of oxygenated and anoxic environments allow N_2O production via both oxidative and reductive pathways. The availability of O_2 is an important factor controlling the rate and pathways of N_2O production in OMZs (Codispoti and Christensen, 1985). The application of ^{15}N tracer

incubation experiments permit the quantitative relationships between O_2 concentration and N_2O production rates and pathways.

4.1.1 N_2O production from NH_4^+ oxidation

The production of N_2O via NH_4^+ oxidation was identified as an important pathway in the OMZ (Cohen and Gordon, 1978). The distribution of rates in the water column of OMZ (Figure 3A) can be explained as follows: (1) In the surface waters (top 30 m), rates of NH_4^+ oxidation to NO_2^- and N_2O are minimal, mainly because NH_4^+ oxidation is suppressed by light (Ward, 2005) and phytoplankton competition for NH_4^+ . (2) Within the oxycline above the ODZ, low O_2 conditions stimulated high rates of N_2O production from NH_4^+ oxidation. This is consistent with O_2 manipulation experiments showing decreased rates of N_2O production from NH_4^+ oxidation with increasing O_2 concentration (Figure 6A). (3) In the anoxic layer below the oxic-anoxic interface, NH_4^+ oxidation is inhibited, resulting in very low or undetectable rates of N_2O production from NH_4^+ oxidation. (4) At deeper depths below the ODZ (generally > 500 m), low population density of ammonia oxidizer and low NH_4^+ availability probably limits NH_4^+ oxidation rate (Peng *et al.*, 2016).

In oxygenated waters ($> 50 \mu M O_2$), the measured N_2O yield of microbial assemblages in ETSP and ETNP (0.003 – 0.06 %) is somewhat similar to those recently measured in cultures of marine ammonia oxidizing bacteria (Frame and Casciotti, 2010) and archaea (Santoro *et al.*, 2011; Löscher *et al.*, 2012; Qin *et al.*, 2017), and is consistent with field measurements outside of OMZ (Yoshida *et al.*, 1989; Grundle *et al.*, 2012). Under suboxic condition ($[O_2] < 5 \mu M$), this and a previous study (Ji *et al.*, 2015) showed N_2O yield $> 1\%$, which is much higher than any yield measured from archaea but close to bacterial yields (Goreau *et al.*, 1980; Frame and Casciotti, 2010). The empirical relationship of N_2O yield vs. O_2 concentration presented here showed that outside of OMZ, the N_2O yield is potentially 2 – 10 fold lower than previously proposed (Nevison *et al.*, 2003), which caused

overestimation of global oceanic N₂O production from nitrification in some earlier studies (Bianchi *et al.*, 2012; Suntharalingam *et al.*, 2012). Within the OMZ, denitrification is the dominant N₂O production pathway (see section 4.1.2); thus when estimating N₂O production via nitrification in OMZ, the error caused by overestimation of N₂O yield could be negligible.

4.1.2 N₂O production from NO₂⁻ and NO₃⁻ reduction

In the anoxic and the peripheral suboxic waters (generally < 10 μM O₂), our ¹⁵N tracer incubation experiments showed that denitrification is the dominant source of N₂O production, because rates of N₂O production from NO₂⁻ and NO₃⁻ reduction were 10 – 100-fold higher than N₂O production from NH₄⁺ oxidation. Similarly, using N₂O natural abundance isotopes, a recent study concluded that incomplete denitrification caused N₂O supersaturation in the Peruvian OMZ (Bourbonnais *et al.*, 2017). Highest rates of N₂O production from NO₂⁻ and NO₃⁻ reduction occurred just below the oxic-anoxic interface, where O₂ inhibition of denitrification is relieved and availability of organic matter promotes denitrification. Rates of N₂O production from NO₂⁻ and NO₃⁻ reduction were higher at the coastal stations than at the offshore stations (Figure 6). This was likely due to higher organic matter content in the coastal waters resulting from higher particle flux, stimulating the growth of denitrifiers and thus, denitrification (Ward *et al.*, 2008; Babbin *et al.*, 2014). Both NO₂⁻ and NO₃⁻ are substrates for denitrifiers producing N₂O. The ratio of rates of the two production pathways is apparently related to the ratio of NO₂⁻ and NO₃⁻ concentrations (Figure 5). Therefore, high NO₃⁻ availability in the water column (Figure S1) probably resulted in higher N₂O production rates from NO₃⁻ than from NO₂⁻. Furthermore, production of N₂O from NO₃⁻ reduction is a series of enzymatic processes, with NO₂⁻ as an intermediate, occurring inside denitrifying cells. The exchange of NO₂⁻ across cell membranes appears to be limited; and the coupling of NO₃⁻ reduction by denitrifiers and NO₂⁻ reduction by nitrifiers seems unlikely (Ji *et al.*, 2015;

Trimmer *et al.*, 2016). The reduction of NO_3^- to NO_2^- ($0 - 20 \text{ nM-N d}^{-1}$, data not shown) could lower the ^{15}N fraction of NO_2^- ($0.4 \text{ }\mu\text{M}$ added) by $\sim 5\%$, which has minimal effect on rate calculation for N_2O production from NO_2^- . The production of N_2O from NO_2^- reduction, particularly in oxygenated waters, can be attributed to nitrifier-denitrification. Rates of NO_2^- reduction to N_2O measured above the oxic-anoxic interface were $0 - 0.5 \text{ nmol-N L}^{-1} \text{ d}^{-1}$, similar to rates measured in the peripheral suboxic waters in the ETNP (Trimmer *et al.*, 2016).

Quantitative relationships between O_2 concentration and rates of N_2O production from NO_2^- and NO_3^- reduction can be described with half inhibition O_2 concentration (C_{50}). The C_{50} for NO_2^- reduction to N_2O in this study ($0.6 - 2.4 \text{ }\mu\text{M}$) is somewhat higher than previously reported in the ETSP ($C_{50} = 0.30 \pm 0.14 \text{ }\mu\text{M}$) (Dalsgaard *et al.*, 2014). By contrast, the C_{50} for NO_3^- reduction to N_2O is 10-fold higher ($14 \pm 4 \text{ }\mu\text{M}$). Although N_2O production from NO_3^- reduction at $> 7 \text{ }\mu\text{M O}_2$ was not tested, rates are expected to decrease at higher O_2 concentrations. In the step-wise denitrification pathway, the enzymes nitrate reductase and nitrite reductase are progressively less oxygen-tolerant (Körner and Zumft, 1989). Thus O_2 inhibition of denitrifying enzymes should render denitrification as an insignificant pathway in oxygenated waters outside of OMZ.

4.2 Model evaluation for global oceanic N_2O flux

With the new quantitative relationships of oxygen and N_2O production from nitrification and denitrification, and sensitivity analyses of nitrification and denitrification parameters, we estimate global oceanic N_2O efflux of $1.7 - 4.4 \text{ Tg-N yr}^{-1}$. Production of N_2O outside of OMZs is attributed to nitrification, and denitrification is the dominant pathway in the OMZ. As denitrification in the OMZs contributes 20 % of total oceanic fluxes, denitrification should be regarded as a net N_2O production pathway on a global perspective. Occupying $< 1 \%$ of global ocean volume, the OMZs of the Eastern Tropical Pacific had intense N_2O fluxes,

equivalent to $0.9 - 9 \text{ mmol-N m}^{-2} \text{ yr}^{-1}$, which is within the range of previous flux estimates of $0 - 13 \text{ mmol-N m}^{-2} \text{ yr}^{-1}$ in the ETSP and ETNP (Cohen and Gordon, 1978; Charpentier *et al.*, 2010). The production of N_2O parameterized in this study depends fundamentally on export and remineralization, therefore the relatively lower export production of this model ($\sim 6 \text{ Pg C yr}^{-1}$) resulted lower N_2O production compared to previous studies (Bianchi *et al.*, 2012; Suntharalingam *et al.*, 2012; Battaglia and Joos, 2018). Statistical analysis shows that our median estimate of annual global production, 2.8 Tg-N yr^{-1} best reproduces the water column and surface N_2O distribution that are currently available (Figure S2). The oxygen-dependent N_2O production rates presented here could be implemented into higher resolution models in future studies constraining highly variable N_2O fluxes in hypoxic coastal zones (Arevalo-Martinez *et al.*, 2015; Capelle *et al.*, 2018). This study suggests 15 % of the global N_2O emission from oceanic contribution, which is lower than IPCC's estimate of 21 % (Ciais *et al.*, 2013). Thus the global N_2O budget could have a relatively greater contribution from anthropogenic activities on land and coastal environments to global N_2O emissions.

The increased N_2O production rates at low oxygen condition suggests that the ongoing ocean de-oxygenation (thickening and horizontal expansion of ODZs, as well as shoaling of the upper oxycline, Stramma *et al.* (2008) could possibly increase future marine N_2O efflux from the OMZs (Codispoti, 2010). By the end of 21st century, it is predicted that the Pacific Ocean will increase the OMZ volume up to 10 % (Cabr e *et al.*, 2015), which will likely result in larger volume of suboxic water for net N_2O production from denitrification. Shoaling of the oxycline allows more rapid exchange between N_2O -supersaturated water and the atmosphere. It is still an open question whether the global oceanic N_2O flux will increase with the ongoing ocean warming. On one hand, warming of the surface ocean lowers N_2O solubility, leading to less N_2O retained in seawater during production, and thus to increased oceanic N_2O emissions. On the other hand, the global oceanic primary production would

decrease and cause lower water column remineralization and thus, lower N₂O production (Martinez-Rey *et al.*, 2015; Landolfi *et al.*, 2017). Experimental approaches to quantify the effect of organic matter availability on N₂O production rates and pathways could facilitate predicting future oceanic N₂O emissions.

5 Conclusion

In the vicinity of water column oxic-anoxic interface within the OMZs of the Eastern tropical Pacific, active N₂O production was measured via oxidative (NH₄⁺ oxidation) and reductive pathways (NO₂⁻ and NO₃⁻ reduction). Production of N₂O from NH₄⁺ oxidation occurred in the oxygenated waters, with higher rates at lower in situ oxygen concentrations. The N₂O yield during nitrification increases with decreasing oxygen concentrations; and the field measurements of N₂O yield were much lower (by 2 – 10-fold) than those from culture experiments. Reduction of NO₂⁻ and NO₃⁻ to N₂O mainly occurred in the anoxic layer and suboxic zones ([O₂] < 5 μM) above the anoxic layer. Production of N₂O via the reductive pathways had much higher rates than that of oxidative pathway. Increasing oxygen concentrations (up to 7 μM) significantly inhibited NO₂⁻ reduction to N₂O; however, NO₃⁻ reduction to N₂O was not effectively inhibited. The relative abundance of water column NO₃⁻ and NO₂⁻ positively correlated with relative rates of N₂O production from respective substrates. In all, denitrification, particularly NO₃⁻ reduction is the dominating N₂O production pathway in the OMZ and adjacent suboxic waters.

We quantified the effects of oxygen concentration on N₂O production from both oxidative and reductive pathways, and implemented into a global ocean model and estimated global oceanic N₂O flux of 1.7 – 4.4 Tg-N yr⁻¹. Although OMZs occupy a small fraction of ocean volume, high rates of N₂O production from denitrification result in OMZs contributed 20 % of oceanic N₂O source. Thus, denitrification should be viewed as a net N₂O production pathway on a global perspective.

Acknowledgments

The authors would like to thank B. Widner and P. Bernhardt for providing seawater nutrient analysis; G. Alarcón for the PPS operations and the STOX sensor data on R/V Atlantis; M. Blum for the PPS operations on R/V Ronald H. Brown and M. Mulholland as chief scientist on R/V Atlantis and Ronald H. Brown. During laboratory analysis, S. Oleynik provided valuable assistance. This research was supported by US-NSF grants OCE-1356043 to B. B. Ward, A. Jayakumar and M. Mulholland. Erik Buitenhuis and Parvatha Suntharalingam acknowledge support from the EU H2020 CRESCENDO project. The authors declare no competing financial interests. The manuscript is prepared to comply with AGU data policy. The data reported in this study can be found in the supplementary dataset.

References

- Arevalo-Martinez, D. L., Kock, A., Loscher, C. R., Schmitz, R. A., & Bange, H. W. (2015). Massive nitrous oxide emissions from the tropical south pacific ocean, *Nature Geosciences*, 8(7), 530-533. <https://doi.org/10.1038/ngeo2469>
- Babbin, A. R., Keil, R. G., Devol, A. H., & Ward, B. B. (2014). Organic matter stoichiometry, flux, and oxygen control nitrogen loss in the ocean, *Science*, 344(6182), 406-408. <https://doi.org/10.1126/science.1248364>
- Babbin, A. R., Bianchi, D., Jayakumar, A., & Ward, B. B. (2015). Rapid nitrous oxide cycling in the suboxic ocean, *Science*, 348(6239), 1127-1129. <https://doi.org/10.1126/science.aaa8380>
- Battaglia, G., & Joos, F. (2018). Marine n₂o emissions from nitrification and denitrification constrained by modern observations and projected in multimillennial global warming simulations, *Global Biogeochemical Cycles*, 32(1), 92-121. doi:10.1002/2017GB005671
- Bianchi, D., Dunne, J. P., Sarmiento, J. L., & Galbraith, E. D. (2012). Data-based estimates of suboxia, denitrification, and n₂o production in the ocean and their sensitivities to dissolved o₂, *Global Biogeochemical Cycles*, 26(2), 6550–6555. <https://doi.org/10.1029/2011GB004209>
- Bisson, K. M., Siegel, D. A., DeVries, T., Cael, B. B., & Buesseler, K. O. (2018). How dataset characteristics influence ocean carbon export models, *Global Biogeochemical Cycles*, 0(32). doi:10.1029/2018GB005934
- Blasing, T. J. (2016). Recent greenhouse gas concentrations, Environmental System Science Data Infrastructure for a Virtual Ecosystem; Carbon Dioxide Information Analysis Center (CDIAC), Oak Ridge National Laboratory (ORNL), Oak Ridge, TN (United States), United States. 10.3334/CDIAC/atg.032
- Bourbonnais, A., Letscher, R. T., Bange, H. W., Échevin, V., Larkum, J., Mohn, J., et al. (2017). N₂o production and consumption from stable isotopic and concentration data in the peruvian coastal upwelling system, *Global Biogeochemical Cycles*, 31(4), 678-698. <https://doi.org/10.1002/2016GB005567>
- Buitenhuis, E. T., Suntharalingam, P., & Le Quéré, C. (2018). Constraints on global oceanic emissions of n₂o from observations and models, *Biogeosciences*, 15(7), 2161-2175.
- Cabré, A., Marinov, I., Bernardello, R., & Bianchi, D. (2015). Oxygen minimum zones in the tropical pacific across cmip5 models: Mean state differences and climate change trends, *Biogeosciences*, 12(18), 5429-5454.
- Capelle, D. W., Hawley, A. K., Hallam, S. J., & Tortell, P. D. (2018). A multi-year time-series of n₂o dynamics in a seasonally anoxic fjord: Saanich inlet, british columbia, *Limnology and Oceanography*, 63(2), 524-539. doi:10.1002/lno.10645
- Charpentier, J., Farías, L., & Pizarro, O. (2010). Nitrous oxide fluxes in the central and eastern south pacific, *Global Biogeochemical Cycles*, 24(3). <https://doi.org/10.1029/2008gb003388>

Ciais, P., C. Sabine, G. Bala, L. Bopp, V. Brovkin, J. Canadell, et al. (2013), Carbon and other biogeochemical cycles, 465–570 pp, Cambridge, United Kingdom and New York, NY, USA.
<https://doi.org/10.1017/CBO9781107415324.015>.

Codispoti, L. A. (2010). Interesting times for marine n_2o , *Science*, 327(5971), 1339-1340.
<https://doi.org/10.1126/science.1184945>

Codispoti, L. A., & Christensen, J. P. (1985). Nitrification, denitrification and nitrous oxide cycling in the eastern tropical south pacific ocean, *Marine Chemistry*, 16(4), 277-300. [https://doi.org/10.1016/0304-4203\(85\)90051-9](https://doi.org/10.1016/0304-4203(85)90051-9)

Codispoti, L. A., Brandes, J. A., Christensen, J. P., Devol, A. H., Naqvi, S. W. A., Paerl, H. W., & Yoshinari, T. (2001). The oceanic fixed nitrogen and nitrous oxide budgets: Moving targets as we enter the anthropocene?, *Scientia Marina*, 65(S2), 85-105.

Cohen, Y., & Gordon, L. I. (1978). Nitrous oxide in the oxygen minimum of the eastern tropical north pacific: Evidence for its consumption during denitrification and possible mechanisms for its production, *Deep-Sea Research*, 25(6), 509-524. [https://doi.org/10.1016/0146-6291\(78\)90640-9](https://doi.org/10.1016/0146-6291(78)90640-9)

Dalsgaard, T., Stewart, F. J., Thamdrup, B., De Brabandere, L., Revsbech, N. P., Ulloa, O., et al. (2014). Oxygen at nanomolar levels reversibly suppresses process rates and gene expression in anammox and denitrification in the oxygen minimum zone off northern chile, *mBio*, 5(6). <https://doi.org/10.1128/mBio.01966-14>

Elkins, J. W., Steven C. Wofsy, Michael B. Mcelroy, Charles E. Kolb, & Kaplan, W. A. (1978). Aquatic sources and sinks for nitrous oxide, *Nature*, 275(5681), 602-606. <https://doi.org/10.1038/275602a0>

Frame, C. H., & Casciotti, K. L. (2010). Biogeochemical controls and isotopic signatures of nitrous oxide production by a marine ammonia-oxidizing bacterium, *Biogeosciences*, 7(9), 2695-2709.
<https://doi.org/10.5194/bg-7-2695-2010>

Freing, A., Wallace, D. W., & Bange, H. W. (2012). Global oceanic production of nitrous oxide, *Philosophical transactions of the Royal Society of London. Series B, Biological sciences*, 367(1593), 1245-1255.
<https://doi.org/10.1098/rstb.2011.0360>

Freing, A., Wallace, D. W. R., Tanhua, T., Walter, S., & Bange, H. W. (2009). North atlantic production of nitrous oxide in the context of changing atmospheric levels, *Global Biogeochemical Cycles*, 23(4).
doi:10.1029/2009GB003472

Garcia, H. E., & Gordon, L. I. (1992). Oxygen solubility in seawater: Better fitting equations, *Limnology and Oceanography*, 6(37), 1307-1312.

Goreau, T. J., Kaplan, W. A., Wofsy, S. C., McElroy, M. B., Valois, F. W., & Watson, S. W. (1980). Production of no_2^- and n_2o by nitrifying bacteria at reduced concentrations of oxygen, *Applied and Environmental Microbiology*, 40(3), 526-532.

Grundle, D. S., Maranger, R., & Juniper, S. K. (2012). Upper water column nitrous oxide distributions in the northeast subarctic pacific ocean, *Atmosphere-Ocean*, 50(4), 475-486. 10.1080/07055900.2012.727779

Hansen, H. P., & Koroleff, F. (1999), *Determination of nutrients*, Wiley-VCH Verlag GmbH, Wiley-VCH Verlag GmbH, Weinheim, Germany.

Holmes, R. M., Aminot, A., Kerouel, R., Hooker, B. A., & Peterson, B. J. (1999). A simple and precise method for measuring ammonium in marine and freshwater ecosystems, *Canadian Journal of Fisheries and Aquatic Sciences*(56), 1801-1808. <https://doi.org/10.1139/f99-128> (1999)

Ji, Q., Babbin, A. R., Jayakumar, A., Oleynik, S., & Ward, B. B. (2015). Nitrous oxide production by nitrification and denitrification in the eastern tropical south pacific oxygen minimum zone, *Geophysical Research Letters*, 42(24), 10,755-710,764. <https://doi.org/10.1002/2015GL066853>

- Kock, A., & Bange, H. W. (2015). Counting the ocean's greenhouse gas emissions, *Eos*(96), 10-13. <https://doi.org/10.1029/2015EO023665>
- Körner, H., & Zumft, W. G. (1989). Expression of denitrification enzymes in response to the dissolved oxygen level and respiratory substrate in continuous culture of *Pseudomonas stutzeri*, *Applied and Environmental Microbiology*, *55*(7), 1670-1676.
- Landolfi, A., Somes, C. J., Koeve, W., Zamora, L. M., & Oschlies, A. (2017). Oceanic nitrogen cycling and N_2O flux perturbations in the anthropocene, *Global Biogeochemical Cycles*, *31*(8), 1236-1255. doi:10.1002/2017GB005633
- Law, C. S., & Owens, N. J. P. (1990). Significant flux of atmospheric nitrous oxide from the northwest Indian ocean, *Nature*, *346*(6287), 826-828. <https://doi.org/10.1038/346826a0>
- Le Quéré, C., Buitenhuis, E. T., Moriarty, R., Alvain, S., Aumont, O., Bopp, L., et al. (2016). Role of zooplankton dynamics for southern ocean phytoplankton biomass and global biogeochemical cycles, *Biogeosciences*, *13*(14), 4111-4133. <https://doi.org/10.5194/bg-13-4111-2016>
- Löscher, C. R., Kock, A., Könneke, M., LaRoche, J., Bange, H. W., & Schmitz, R. A. (2012). Production of oceanic nitrous oxide by ammonia-oxidizing archaea, *Biogeosciences*, *9*(7), 2419-2429. <https://doi.org/10.5194/bg-9-2419-2012>
- Madec, G., Delecluse, P., Imbard, M., & Lévy, C. (1998), Opa 8.1 ocean general circulation model reference manual, notes pole model, edited by I. P. S. L. d. S. d. I. E. Global, p. 91, Laboratoire d'Océanographie DYnamique et de Climatologie.
- Martinez-Rey, J., Bopp, L., Gehlen, M., Tagliabue, A., & Gruber, N. (2015). Projections of oceanic N_2O emissions in the 21st century using the IPSL earth system model, *Biogeosciences*, *12*(13), 4133-4148. 10.5194/bg-12-4133-2015
- McIlvin, M. R., & Altabet, M. A. (2005). Chemical conversion of nitrate and nitrite to nitrous oxide for nitrogen and oxygen isotopic analysis in freshwater and seawater, *Analytical Chemistry*, *77*(17), 5589-5595.
- Nevison, C., Butler, J. H., & Elkins, J. W. (2003). Global distribution of N_2O and the $\delta^{15}\text{N}$ - N_2O -aou yield in the subsurface ocean, *Global Biogeochemical Cycles*, *17*(4). <https://doi.org/10.1029/2003GB002068>
- Peng, X., Fuchsman, C. A., Jayakumar, A., Warner, M. J., Devol, A. H., & Ward, B. B. (2016). Revisiting nitrification in the eastern tropical south Pacific: A focus on controls, *Journal of Geophysical Research: Oceans*, *121*(3), 1667-1684. 10.1002/2015JC011455
- Poth, M., & Focht, D. D. (1985). ^{15}N kinetic analysis of N_2O production by *Nitrosomonas europaea*: An examination of nitrifier denitrification, *Applied and Environmental Microbiology*, *49*(5), 1134-1141.
- Prather, M. J., Holmes, C. D., & Hsu, J. (2012). Reactive greenhouse gas scenarios: Systematic exploration of uncertainties and the role of atmospheric chemistry, *Geophysical Research Letters*, *39*(9). <https://doi.org/10.1029/2012GL051440>
- Qin, W., Meinhardt, K. A., Moffett, J. W., Devol, A. H., Virginia Armbrust, E., Ingalls, A. E., & Stahl, D. A. (2017). Influence of oxygen availability on the activities of ammonia-oxidizing archaea, *Environmental Microbiology Reports*, *9*(3), 250-256. <https://doi.org/10.1111/1758-2229.12525>
- Ravishankara, A., Daniel, J. S., & Portmann, R. W. (2009). Nitrous oxide (N_2O): The dominant ozone-depleting substance emitted in the 21st century, *Science*, *326*(5949), 123-125.
- Revsbech, N. P., Larsen, L. H., Gundersen, J., Dalsgaard, T., Ulloa, O., & Thamdrup, B. (2009). Determination of ultra-low oxygen concentrations in oxygen minimum zones by the Stox sensor, *Limnology and Oceanography Methods*, *7*, 371-381.
- Santoro, A. E., Buchwald, C., McIlvin, M. R., & Casciotti, K. L. (2011). Isotopic signature of N_2O produced by marine ammonia-oxidizing archaea, *Science*, *333*(6047), 1282-1285. <https://doi.org/10.1126/science.1208239>

Siegel, D. A., Buesseler, K. O., Doney, S. C., Sailley, S. F., Behrenfeld, M. J., & Boyd, P. W. (2014). Global assessment of ocean carbon export by combining satellite observations and food-web models, *Global Biogeochemical Cycles*, 28(3), 181-196. doi:10.1002/2013GB004743

Stramma, L., Johnson, G. C., Sprintall, J., & Mohrholz, V. (2008). Expanding oxygen-minimum zones in the tropical oceans, *Science*, 320(5876), 655-658. https://doi.org/10.1126/science.1153847

Suntharalingam, P., Buitenhuis, E., Le Quéré, C., Dentener, F., Nevison, C., Butler, J. H., et al. (2012). Quantifying the impact of anthropogenic nitrogen deposition on oceanic nitrous oxide, *Geophysical Research Letters*, 39(7). https://doi.org/10.1029/2011GL050778

Takahashi, T., Broecker, W. S., & Langer, S. (1985). Redfield ratio based on chemical data from isopycnal surfaces, *Journal of Geophysical Research: Oceans*, 90(C4), 6907-6924. https://doi.org/10.1029/JC090iC04p06907

Trimmer, M., Chronopoulou, P.-M., Maanoja, S. T., Upstill-Goddard, R. C., Kitidis, V., & Purdy, K. J. (2016). Nitrous oxide as a function of oxygen and archaeal gene abundance in the north pacific, *Nature Communications*, 7, 13451. https://doi.org/10.1038/ncomms13451

UNESCO (1994), Protocols for the joint global ocean flux study (jgofs) core measurements, edited by I. O. Commission, United Nations Educational, Scientific and Cultural Organization.

Wanninkhof, R. (1992). Relationship between wind speed and gas exchange over the ocean, *Journal of Geophysical Research: Oceans*, 97(C5), 7373-7382. https://doi.org/10.1029/92JC00188

Ward, B. B. (2005). Temporal variability in nitrification rates and related biogeochemical factors in monterey bay, california, USA, *Marine Ecology Progress Series*, 292, 97-109. https://doi.org/10.3354/meps292097

Ward, B. B., Tuit, C. B., Jayakumar, A., Rich, J. J., Moffett, J., & Naqvi, S. W. A. (2008). Organic carbon, and not copper, controls denitrification in oxygen minimum zones of the ocean, *Deep-Sea Research Part I*, 55(12), 1672-1683. https://doi.org/10.1016/j.dsr.2008.07.005

Weiss, R. F., & Price, B. A. (1980). Nitrous oxide solubility in water and seawater, *Marine Chemistry*, 8(4), 347-359. https://doi.org/10.1016/0304-4203(80)90024-9

Wilson, S. T., del Valle, D. A., Segura-Noguera, M., & Karl, D. M. (2014). A role for nitrite in the production of nitrous oxide in the lower euphotic zone of the oligotrophic north pacific ocean, *Deep-Sea Research Part I*, 85, 47-55. https://doi.org/10.1016/j.dsr.2013.11.008

Yoshida, N., Morimoto, H., Hirano, M., Koike, I., Matsuo, S., Wada, E., et al. (1989). Nitrification rates and ¹⁵N abundances of n₂O and no₃⁻ in the western north pacific, *Nature*, 342(6252), 895-897. 10.1038/342895a0

Table 1. Sensitivity analysis of annual global oceanic N₂O production from nitrification and denitrification. Median production was calculated based on median parameterizations for both nitrification and denitrification (simulation 1). The uncertainties for N₂O production from nitrification and denitrification were derived from simulations 2 and 3, and simulation 4 and 5, respectively.

Simulation number	Nitrification yield $J_1 = [a / [O_2] (\mu\text{M}) + b]$	Denitrification $f(O_2) = \exp(\lambda (O_2 (\mu\text{M}) - 1))$	N ₂ O production from nitrification (Tg N yr ⁻¹)	N ₂ O production from denitrification (Tg N yr ⁻¹)	Annual N ₂ O production (Tg N)
1	$a = 0.2, b = 0.08$	$\lambda = -0.1$ (e -folding $[O_2] = 10 \mu\text{M}$)	2.2	0.6	2.8
2	$a = 0.07, b = 0.04$	$\lambda = -0.1$ (e -folding $[O_2] = 10 \mu\text{M}$)	1.1	0.6	1.7
3	$a = 0.33, b = 0.12$	$\lambda = -0.1$ (e -folding $[O_2] = 10 \mu\text{M}$)	3.3	0.6	3.9
4	$a = 0.2, b = 0.08$	$\lambda = -0.6667$ (e -folding $[O_2] = 1.5 \mu\text{M}$)	2.2	0.1	2.3
5	$a = 0.2, b = 0.08$	$\lambda = -0.05$ (e -folding $[O_2] = 20 \mu\text{M}$)	2.2	2.1	4.3

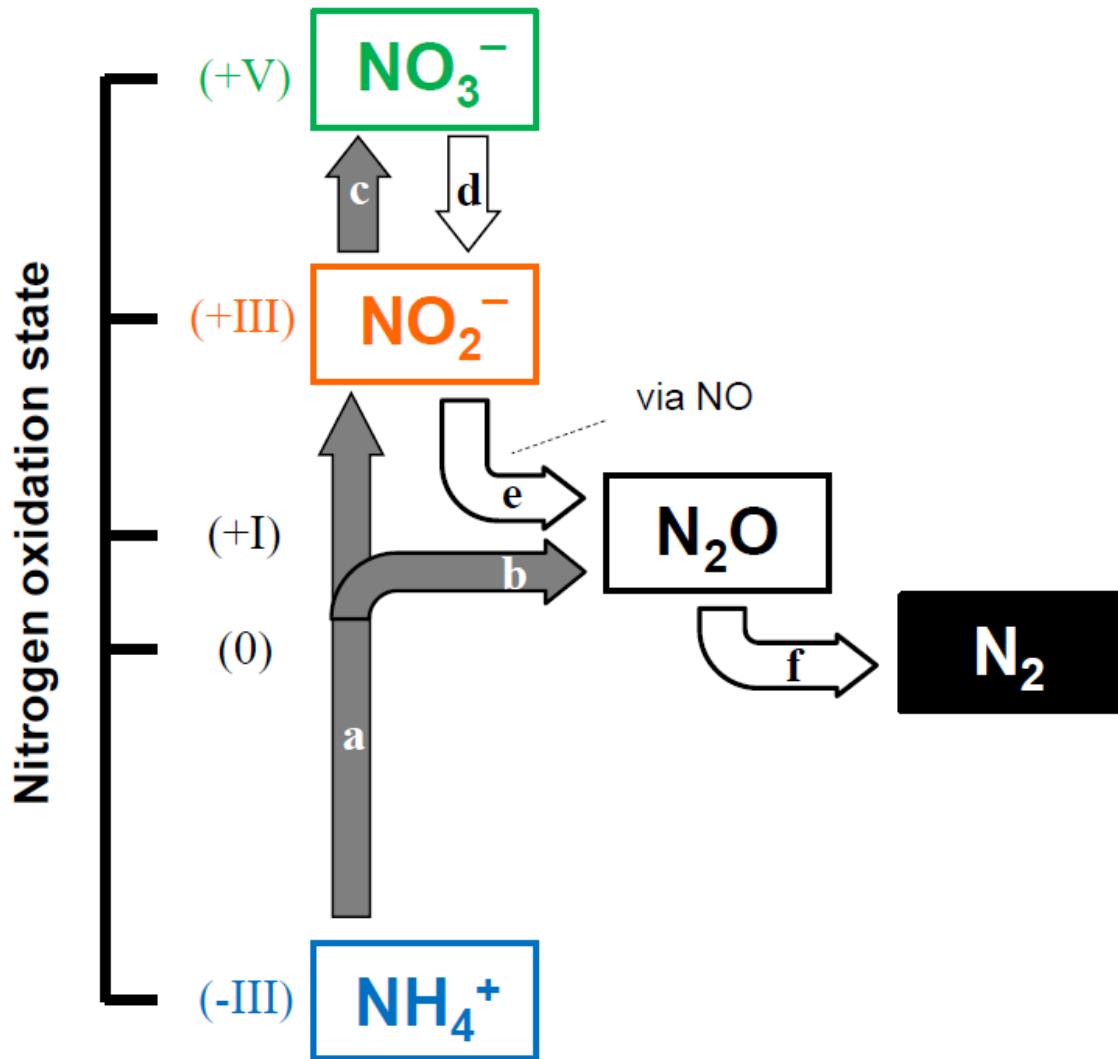


Figure 1. Nitrogen transformations related to N_2O production and consumption in marine environments. (a) Ammonium (NH_4^+) oxidation to nitrite (NO_2^-). (b) NH_4^+ oxidation to N_2O . (c) NO_2^- oxidation to nitrate (NO_3^-). (d) NO_3^- reduction to NO_2^- . (e) NO_2^- reduction to N_2O via nitric oxide (NO). (f) N_2O reduction to N_2 . Filled arrows (reaction (a), (b) and (c)) represent oxidative pathways, requiring molecular oxygen as terminal electron acceptor. Open arrows (reaction (d), (e) and (f)) represent reductive pathways requiring organic matter as the electron donor. In the main text, N_2O production from nitrification includes pathways (b) and (a) coupled with (e); N_2O production from denitrification includes pathways (e) and (d) coupled with (e).

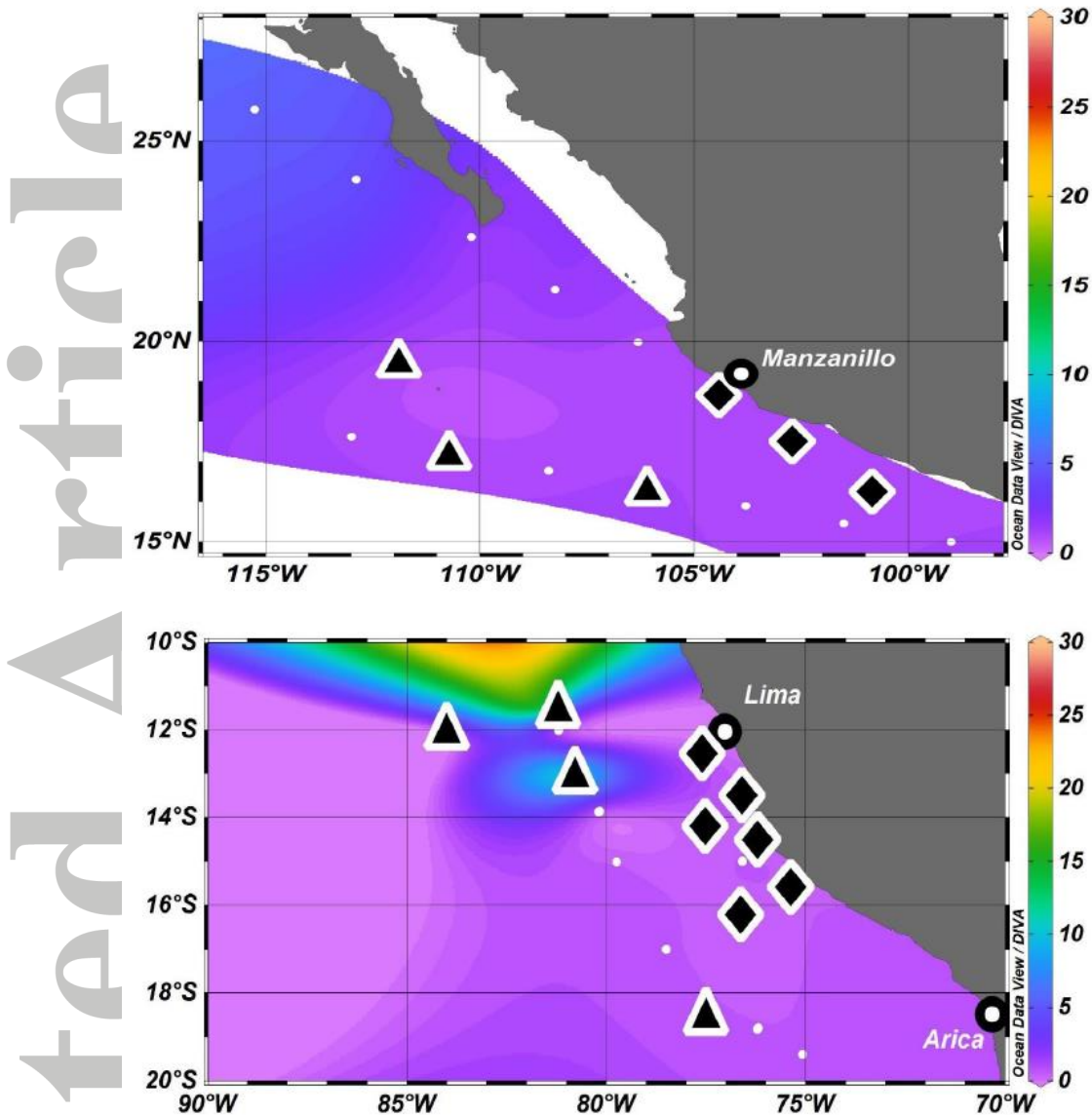


Figure 2. Sampling locations during cruises in 2016 ETNP (upper panel) and 2015 ETSP (lower panel). Comprehensive measurements of nitrous oxide production were performed at stations representing coastal environment (diamonds) and open-ocean environment (triangles). High resolution oxygen profiles were obtained at both comprehensive stations and transect stations (dots). Color map shows minimum dissolved oxygen concentration ($\mu\text{mol L}^{-1}$) within the upper 1000 m water column.

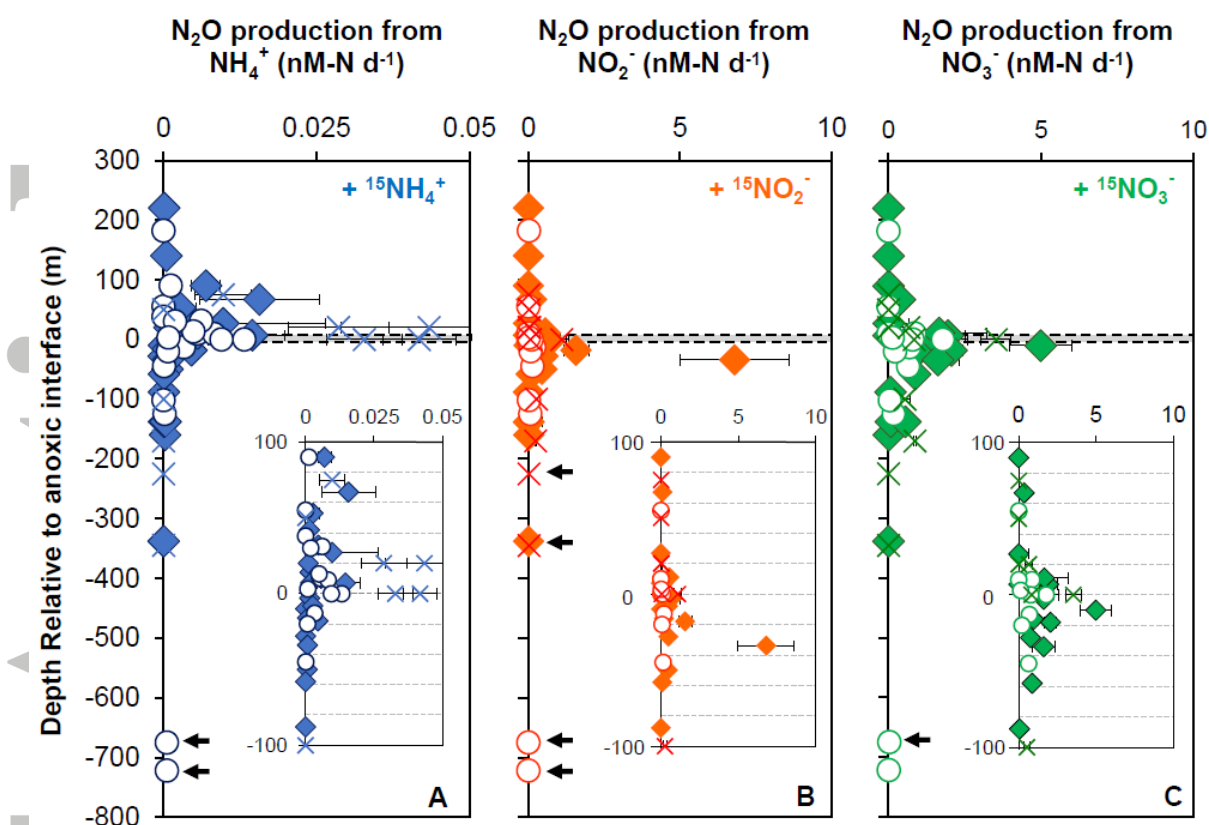


Figure 3. Rates of N_2O production from NH_4^+ oxidation (A), NO_2^- reduction (B) and NO_3^- reduction (C) at depths relative to the oxic-anoxic interface (shaded line) during cruises in 2013 ETSP (crosses), 2015 ETSP (filled diamonds) and 2016 ETNP (open circles). Arrows represent significant ($p < 0.05$, see methods) production rates at depth ≥ 200 m below oxic-anoxic interface. Inset: N_2O production from NH_4^+ oxidation (A), NO_2^- reduction (B) and NO_3^- reduction (C) within ± 100 m of the oxic-anoxic interface. Error bar represents standard deviation of rates derived from a linear fit to three time points measured in duplicate ($n = 5$).

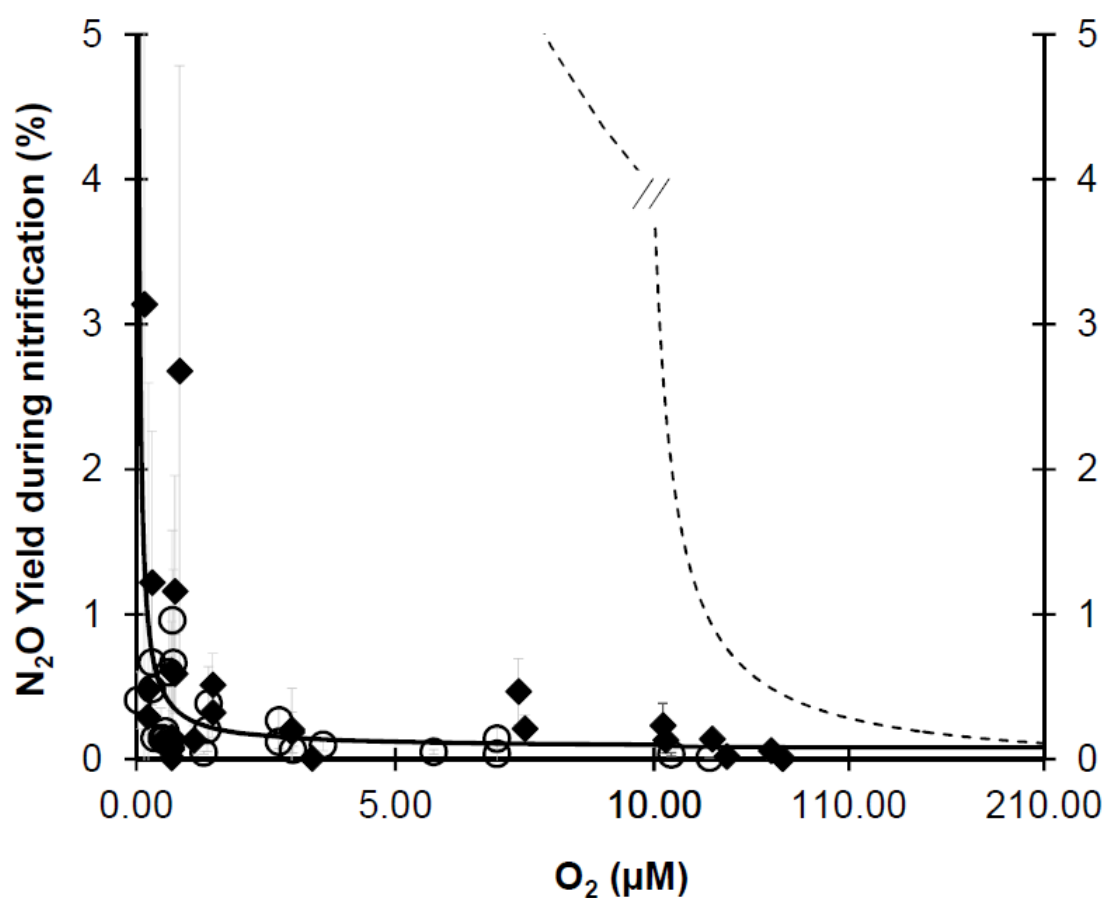


Figure 4. N₂O yield (%) during nitrification, the molar nitrogen ratio of N₂O production to NO₂⁻ production during NH₄⁺ oxidation, measured at a range of O₂ concentrations. Data are from cruises in 2015 ETSP (filled diamonds) and 2016 ETNP (open circles) and compared to the N₂O yield vs. oxygen relationship based on the bacterial culture work (Goreau *et al.*, 1980; Nevison *et al.*, 2003) (dashed line) and the empirical fit in this study (solid line, Yield (%) = 0.2/[O₂] (μM) + 0.08).

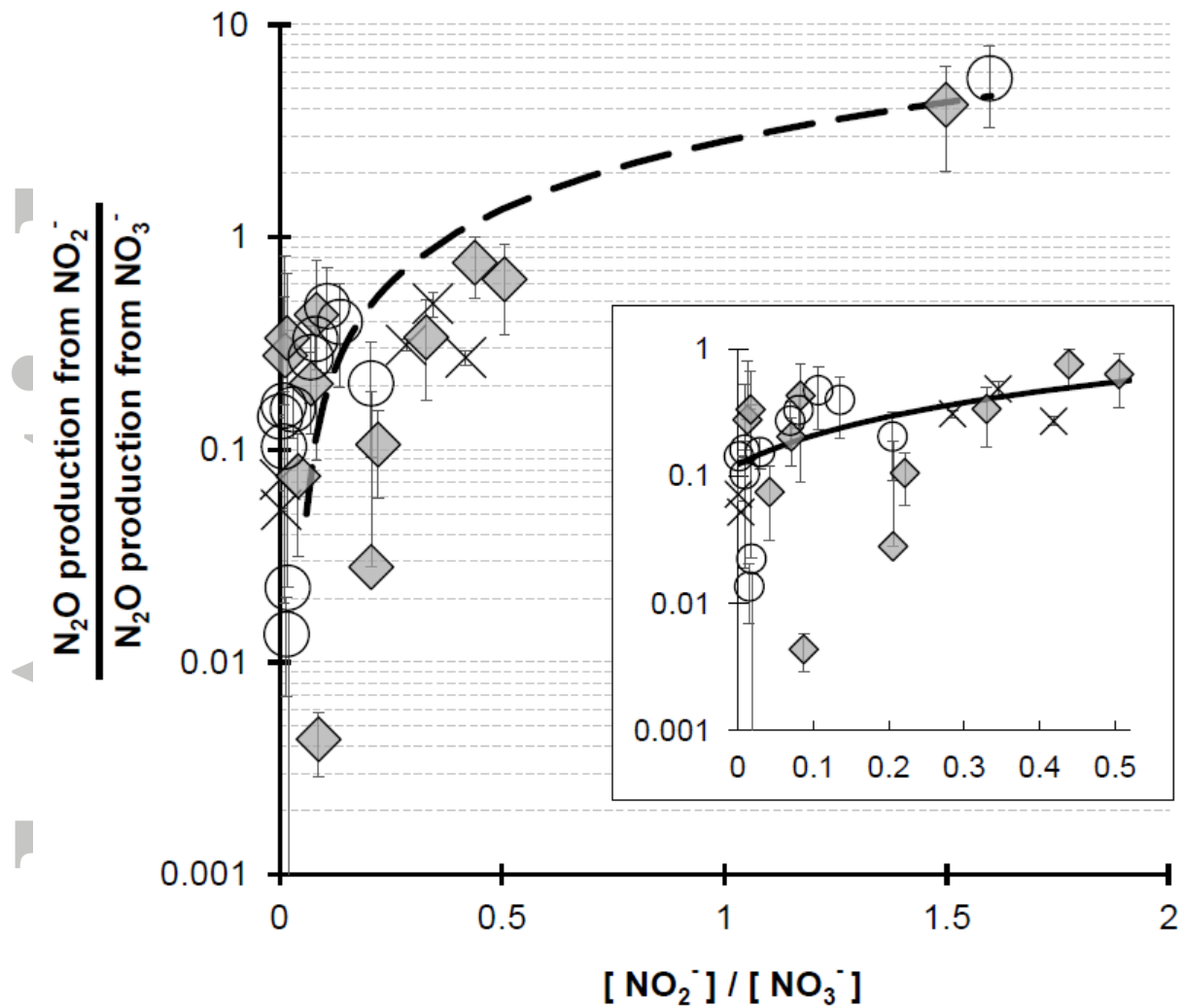


Figure 5. The ratio of N_2O production rates from NO_2^- and that from NO_3^- plotted against ratio of NO_2^- and NO_3^- concentrations during incubation experiments. Only significant production rates are plotted. Data are from cruises of 2013 ETSP (cross), 2015 ETSP (filled diamonds) and 2016 ETNP (circles). Linear regressions were statistically significant for data with NO_2^- and NO_3^- concentration ratios below 0.5 (solid line, inset) and below 1.6 (dashed line). Curvature of linear regression was due to logarithmic scale on y-axis. Inset: Plotted data with NO_2^- and NO_3^- concentration ratio < 0.5 .

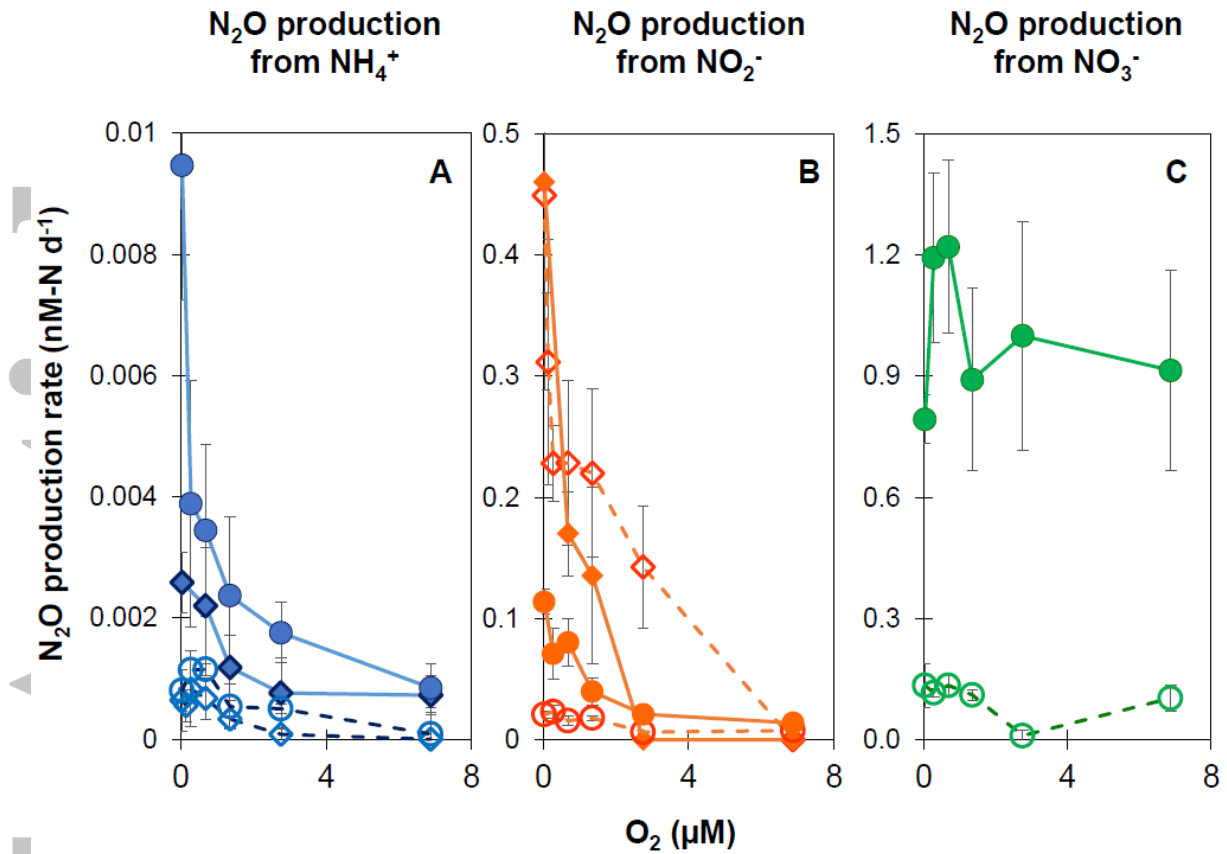


Figure 6. Rates of N_2O production from NH_4^+ oxidation (A), NO_2^- reduction (B) and NO_3^- reduction (C) under manipulated oxygen concentrations during cruises in 2015 ETSP (diamonds) and 2016 ETNP (circles). Measurements were performed at stations representing coastal environment (filled symbols) and open-ocean environment (open symbols). The *in situ* oxygen concentrations at the time of sampling was $< 0.1 \mu M$. Standard deviation of rates derived from a linear fit to three time points measured in duplicate ($n = 5$).

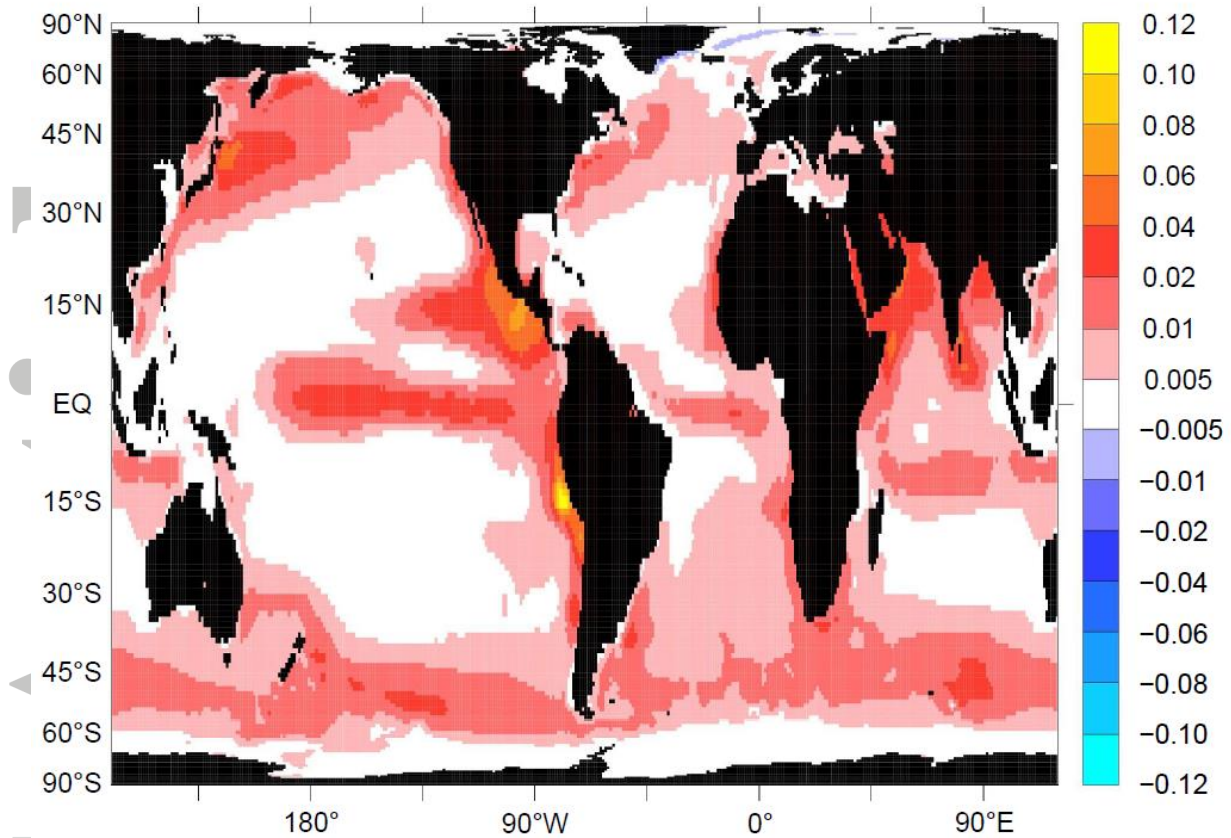


Figure 7. Global ocean N₂O flux (gN m⁻² yr⁻¹, color bar on right) determined by a model simulation. Positive values indicate net flux from the ocean to the atmosphere. Simulation were performed with nitrification parameterization from this study (N₂O yield (%) = 0.2/[O₂]+0.08), and denitrification parameterization of e-folding [O₂] = 10 μM. The result of global oceanic net N₂O production is 2.8×10^{12} g N yr⁻¹.

Accepted